Nonlinear deflection analysis of helical spring in elastic-perfect plastic material: application to the plastic extension of piano wire spring

Hiroyuki Kato[a], Hitoshi Suzuki[b]

[a]*Mechanical and Space Engineering, Hokkaido University, Sapporo 060-8628, Japan*
[b]*Graduate school of Engineering, Hokkaido Univeristy, Japan*

Abstract

A mechanics-of-materials theory of the nonlinear deflection of helical spring within and beyond the elasticity limit was developed. The theory examined the nonlinearity due to the combined stresses of the torsion and bending of spring element by assuming the elastic-perfect plastic material obeying Tresca yield criterion. Free rotation of spring around the spring axis was taken into account. It was shown in experiment that the stress-strain curve of a piano wire was close to elastic-perfect plastic one. The outcome of the theory was compared with the experimental result of nonlinear load-deflection curves in plastically extended helical spring made of a piano wire.
Keywords: Plasticity, Spring, Geometrical nonlinearity, Moving boundary problem, Elliptic integral

Email addresses: hkato@eng.hokudai.ac.jp (Hiroyuki Kato), h.suzuki@frontier.hokudai.ac.jp (Hitoshi Suzuki)

1. Introduction

Flexibility is sometimes needed, and springs are designed to fit designer's needs for carrying load with elastic displacement (Wahl, 1963; Shigley, 2015; Kobelev, 2018). The slope of linear load-deflection relation is given by the conventional formula of spring constant, $k = Gd^4/(8D^3N)$, where d and D are wire and coil radius, N, the number of turns, G, the shear modulus (Love, 1944; Timoshenko and Goodier, 1970).

Nonlinearity would appear in load–deflection relation of helical spring when the deflection becomes large. One origin is the geometrical nonlinearity, which is termed "pitch angle effect" in classical work (Wahl, 1963). Note that the above spring constant is obtained by considering only the torsion of spring element due to external load. This approximation may be correct for small deflection of closely pitched spring. In sparsely pitched springs, however, the deflection due to the bending of spring element cannot be ignored. Moreover, the combined deflection of torsion and bending would occur in any spring when the deflection becomes large.

Another geometrical nonlinearity comes from the free rotation around spring axis. The free rotation has been known to occur (Love, 1944; Wahl, 1963; Timoshenko and Goodier, 1970) and the elasticity analysis was given (Burns, 2011). When the end of spring is fixed not to rotate, a certain amount of torque should be subjected to the end. The magnitude of the torque would increase with increasing the deflection of spring. Present study considered the free-to-rotate end in order to simplify the boundary condition of the analysis.

The other origin is the material's nonlinearity due to plasticity in metals

and alloys. The plasticity of springs is practically used in the cold-setting operation, and the yield criterion was discussed (Wahl, 1963). Since former studies were concerned with the elasticity limit, present study shall derive the load–deflection relation in plastic range. Such theoretical argument of plasticity may be of significance not only because of the advance in continuum mechanics but also possible application to materials capable of restoring large inelastic deflection, such as shape memory alloys (Tobushi and Tanaka, 1991; Mirzaeifar et al., 2011; An et al., 2012; Savi et al., 2015; Koh, 2018) and some kind of polymers. As for modern technology, shape memory polymer micro springs have been fabricated by the novel 3D/4D printing (Ge et al., 2013).

This study examines plasticity under the approximations of (i) no curvature effect in the assumption of large spring index, which is the ratio of spring radius to element wire radius (Wahl, 1963; Shigley, 2015; Kobelev, 2018), and (ii) the elastic-perfect plastic materials. These are for the brevity in developing formula. In principle, any realistic materials can be dealt with by some numerical computation. Present theory may work for giving some perspectives to understand the nonlinear phenomena.

2. Symbols and units

R, D, spring radius and diameter in mm

R_0, D_0, initial coil radius and diameter in mm

ρ, radius of curvature of element in mm

d, element diameter in mm

N, number of turns

ℓ, length of helical element per turn before deflection

δ, deflection per turn in mm

Φ, rotation angle per turn around spring axis in rad. or deg.

φ_T, twisting angle per turn in rad. or deg.

φ_M, bending angle per turn in rad. or deg.

P, load on spring in N

T, torsion moment in N·mm

M, bending moment in N·mm

α, pitch angle in rad.

τ_0, shear stress of perfect plasticity

E, G, modulus of elasticity and shear modulus,

I_y, moment of inertia of area in mm^4

I_p, polar moment of inertia of area in mm^4

$a,\ b$, short and long axes of ellipsoid in mm

c, spring index, $= D/d$

K, curvature correction factor (Wahl, 1963; Timoshenko and Goodier, 1970; Shigley, 2015),

$$K = \frac{4c-1}{4c-4} + \frac{0.615}{c} \quad . \tag{1}$$

k, elastic spring constant (Wahl, 1963; Timoshenko and Goodier, 1970; Shigley, 2015),

$$k = \frac{Gd^4}{8ND_0^3} \quad . \tag{2}$$

3. Analysis

3.1. Geometry of helical spring

As it used to be assumed (Wahl, 1963; Shigley, 2015; Kobelev, 2018), the length of spring element is unchanged during deflection, since the axial strain

is negligibly small. The length per turn in the natural length ℓ is equal to $2\pi R_0$. Figure 1(a) is a helix with the radius R equal to the radius of the tangent cylinder where the element diameter is ignored. The helix line with the pitch angle α in the rectangular O-$x_1x_2x_3$ coordinate is

$$x_1 = R\cos\theta, \quad x_2 = R\sin\theta, \quad x_3 = R\theta\tan\alpha \quad . \tag{3}$$

Since the length of element in $d\theta$ is

$$ds = R\sec\alpha \; d\theta \quad , \tag{4}$$

the length of element of one turn is

$$L = \oint_L ds = 2\pi R\sec\alpha \; . \tag{5}$$

These variables form a triangle (a), which defines the conventional value of the pitch p equal to $L\sin\alpha$.

As illustrated in Fig.1(b), the rotation of the free end of spring occurs during extension (Wahl, 1963; Burns, 2011). The angle Φ is defined along the element of length ℓ as

$$\ell = \int_\ell ds = R\sec\alpha \int_0^{2\pi-\Phi} d\theta \; , \tag{6}$$

or

$$(2\pi - \Phi)R = \ell\cos\alpha \quad . \tag{7}$$

These variables form a triangle (b). Accordingly, the deflection is

$$\delta = \ell\,(\sin\alpha - \sin\alpha_0) \quad . \tag{8}$$

This study deals with closely pitched springs, so that the offset due to the initial pitch angle $\sin\alpha_0$ shall be ignored for brevity.

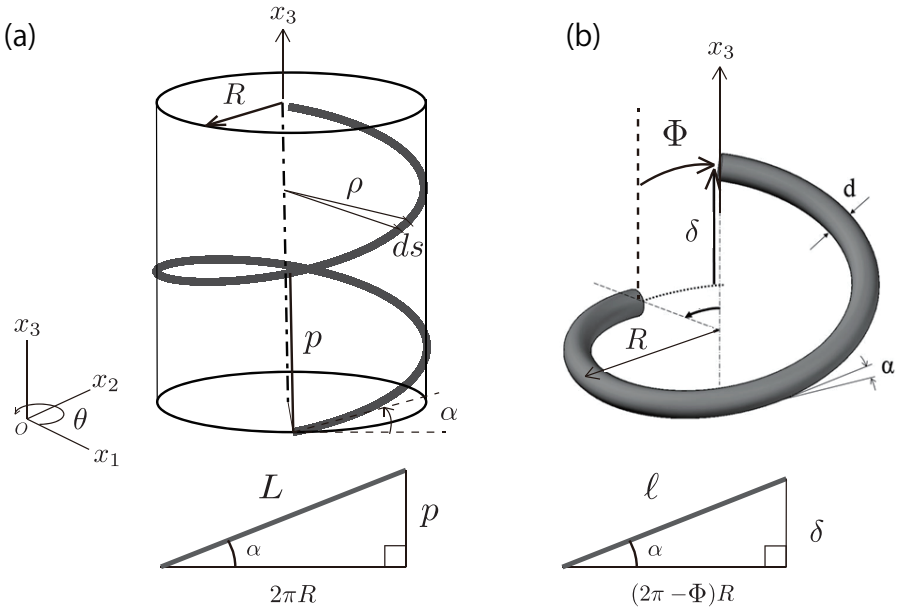

Figure 1: (a) The geometrical parameters of helix line and (b) the rotation of spring element around the spring axis. The angle is positive in the unwinding direction.

The load P forms a moment PR on the wire element. The moment is resolved into the axial components T and the tangential one M (Fig.2),

$$T = -PR\cos\alpha \quad \text{and} \quad M = -PR\sin\alpha \quad . \tag{9}$$

The minus sign is required since the direction in the right hand screw is opposite to the outward normal of the cross section. The same expressions are seen in literatures (Burns, 2011; Kobelev, 2018). Hereafter, the moment $PR = X$ is taken as an independent variable in place of P.

When the spring element is subjected to the twisting (torsion) angle per pitch φ_T, the change in the twist angle along the infinitesimally small length ds is given as $d\varphi_T = (\varphi_T/\ell)ds$. Similarly, when the bending angle per pitch is φ_M, the change in the bending angle is $d\varphi_M = (\varphi_M/\ell)ds$. Then, the changes

in angle tangential and parallel to the coil axis in infinitesimally small length ds are (Fig.2),

$$d\varphi_1 = d\varphi_T \cos\alpha + d\varphi_M \sin\alpha \ , \tag{10}$$

$$d\varphi_2 = -d\varphi_T \sin\alpha + d\varphi_M \cos\alpha \ . \tag{11}$$

These are related to the deflection per pitch and the rotation angle per pitch

$$\delta = -\int R d\varphi_1 \ , \tag{12}$$

$$\Phi = \int d\varphi_2 \ . \tag{13}$$

By integrating these along the pitch, we get

$$\delta = -R(\varphi_T \cos\alpha + \varphi_M \sin\alpha), \tag{14}$$

$$\Phi = -\varphi_T \sin\alpha + \varphi_M \cos\alpha. \tag{15}$$

The simultaneous equations are solved with Eq.7 and 8 have the solutions

$$\varphi_T = -2\pi \sin\alpha, \tag{16}$$

$$\varphi_M = 2\pi \left(\cos\alpha - \frac{R_0}{R} \right). \tag{17}$$

3.2. Elasticity

At the onset of loading, the deflection occurs elastically. In elasticity, the polar area moment of inertia I_p is $\pi d^4/32$ and the area moment of inertia around the y-axis I_y is $\pi d^4/64$. The twist angle per pitch φ_T is given by the elementary elasticity formula

$$\varphi_T = \frac{T\ell}{GI_p} = -\frac{32X\ell\cos\alpha}{\pi G d^4} \ . \tag{18}$$

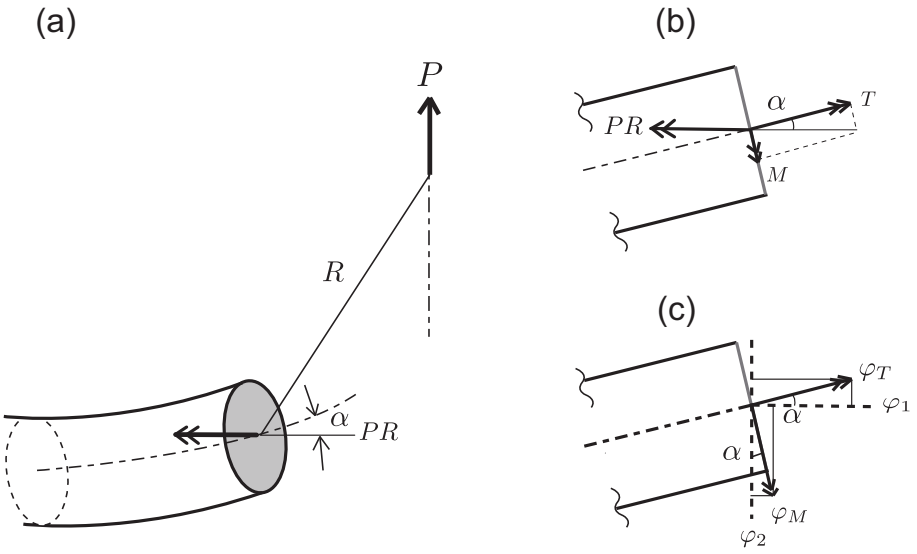

Figure 2: The applied moment PR, (a), the components of torsion moment T and bending M, (b), and the torsion angle φ_T and bending angle φ_M, (c).

By Eq.16, we get

$$X = \frac{\pi^2 G d^4 \tan\alpha}{16\ell} \quad . \tag{19}$$

Next, let us consider the bending of curved beam with the curvature changing from the initial magnitude of $1/\rho_0$ to $1/\rho$ ($\rho > \rho_0$). The curvature is related to the bending moment M and the rigidity EI_y

$$\frac{1}{\rho_0} = \frac{1}{\rho} + \frac{M}{EI_y}, \tag{20}$$

This equation is derived in Appendix A. The pitch angle α and the radius of curvature are related to the spring radius

$$\rho = R\sec\alpha, \tag{21}$$

and $\rho_0 = R_0$. Alternatively, the change in the radius of curvature is related

to the bending angle (see Appendix B)

$$\varphi_M = 2\pi \left(1 - \frac{\rho_0}{\rho}\right). \tag{22}$$

By Eq.20 and 21, we get

$$\varphi_M = \frac{2\pi\rho_0 M}{EI_y} = -\frac{128 R_0 X \sin\alpha}{Ed^4} \ . \tag{23}$$

Equating this to Eq.17, R is obtained by Eq.19,

$$\frac{1}{R} = \frac{\cos\alpha}{R_0}\left(1 + \frac{2G\tan^2\alpha}{E}\right) \ . \tag{24}$$

Once R is known as Eq.24, the load P is determined from Eq.19 through $P = XR^{-1}$. Using the standard expression of the elastic spring constant k of Eq.2, the load vs δ relation is

$$P = k\delta\left(1 + \frac{2G\tan^2\alpha}{E}\right) \quad . \tag{25}$$

This formula modifies the conventional relation $P = k\delta$ to include the pitch angle effect. The pitch angle α is given by δ through Eq. 8. A similar but different form of the formula is seen (Shigley, 2015). The difference is due to the bending term involved in the present analysis.

Next, the rotation angle per turn is by Eq.7

$$\Phi = 2\pi\left(1 - \frac{R_0}{R}\cos\alpha\right) \quad . \tag{26}$$

By Eq.24, we get the expression:

$$\Phi = 2\pi(1 - 2G/E)\sin^2\alpha = \frac{2\pi\nu}{1+\nu}\sin^2\alpha \ . \tag{27}$$

The right side is positive, indicating that the elastic rotation occurs always in the unwinding direction.

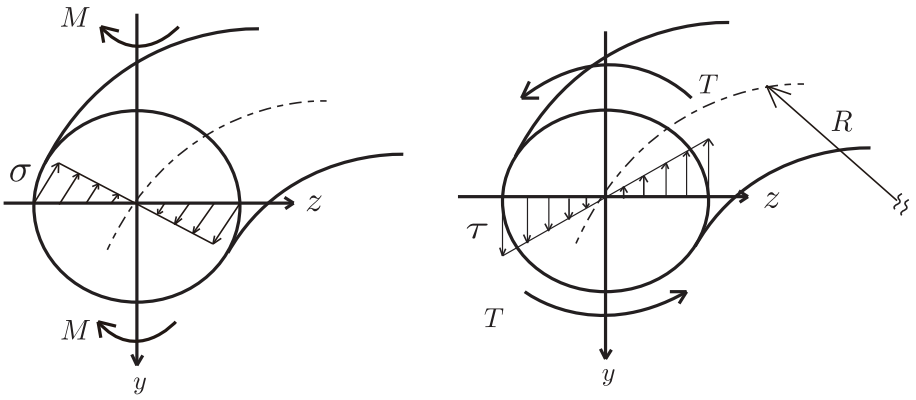

Figure 3: The combined stress-state of bending, (a), and torsion, (b), of the element wire.

3.3. Yield criterion

When the applied stress goes beyond the elasticity limit of wire, plasticity would appear. The plasticity of steels occurs by slip at room temperature and results in permanent plastic strain. The larger the pitch angle α is, the larger the bending moment M becomes. It follows that bending cannot be ignored in the deflection of any spring at large deflection(Wahl, 1963; Shigley, 2015). Then, the shearing stress of torsion τ is combined with the bending stress σ, as illustrated in Fig.3.

Present study takes the z-y rectangular coordinate on the cross section of wire, as shown in Fig.3. The plastic yielding occurs first by torsion, since τ is much larger than σ at the onset of yielding. The Tresca yielding criterion with the equivalent stress of $\tau_0 = Y/2$, where Y is the flow stress in uniaxial tensile testing, is given as

$$\left(\frac{\sigma}{2}\right)^2 + \tau^2 = \tau_0^2 \quad , \tag{28}$$

where the bending stress in elastic range is

$$\sigma = \frac{M}{I_y} z = \frac{2M}{I_p} z \quad , \tag{29}$$

and the shearing stress of torsion is

$$\tau = \frac{T}{I_p} r \quad . \tag{30}$$

Then, the yield locus or the elastic–plastic boundary is an ellipsoid

$$\left(\frac{z}{a}\right)^2 + \left(\frac{y}{b}\right)^2 = 1, \tag{31}$$

where

$$a = \frac{I_p \tau_0}{\sqrt{M^2 + T^2}} = \frac{I_p \tau_0}{X} \quad , \tag{32}$$

$$b = \frac{I_p \tau_0}{T} = \frac{I_p \tau_0 \sec \alpha}{X} \quad . \tag{33}$$

The length of short axis a and that of the long axis b decrease and the axial ratio b/a increases with increasing the moment X.

During elastic deformation the yield locus is outside the cross section, as illustrated in Fig.4(a). The yielding occurs when the a-axis touches the outer surface, such that $a = d/2$, as in Fig.4(b). It occurs when the moment is at the critical magnitude.

$$X^* = \frac{\pi d^3 \tau_0}{16} \quad . \tag{34}$$

As deflected further, the ellipsoid is inside in the cross section. It occurs when the long axis b is shorter than the radius $d/2$, as in Fig.4(c). The critical moment is $X^{**} = X^* \sec \alpha$.

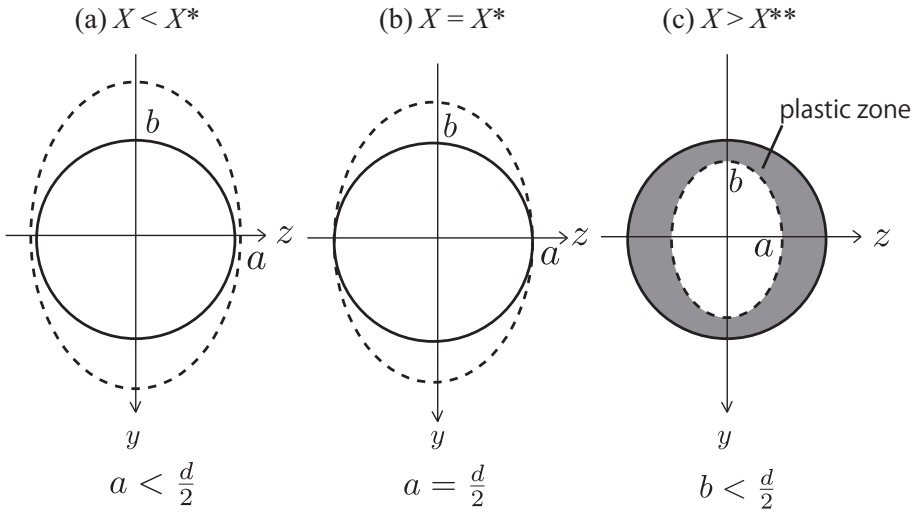

Figure 4: Schematic drawings of the development of yield surface of plasticity. The yield locus is outside the cross-section area in (a), attached to the outer surface in (b), and inside the area in (c).

3.4. Plastic torsion

When $X > X^*$, the torque T acting on the element is the sum of the elastic torque T_e and the plastic torque T_p

$$T = T_e + T_p \quad . \tag{35}$$

This relation has been originally suggested by Wahl (1963). Present analysis shall gives further discussion. Let the torsion angle per pitch be φ_T and the elastic torque acting on the area inside the ellipsoid is

$$T_e = \frac{1}{\ell}\int_{in} G\varphi_T r^2 dA = \frac{G\varphi_T}{\ell}\int_{in} r^2 dA = \frac{G\varphi_T}{\ell}\tilde{I}_p \quad , \tag{36}$$

where the polar area moment of inertia $\tilde{I}_p$ of the ellipsoid is

$$\tilde{I}_p = \pi\frac{a^3 b^3}{a^2 + b^2}. \tag{37}$$

The plastic torsion occurs on the section outside the ellipsoid.

$$T_p = -\int_{out} \tau r dA = 4\int_0^{\pi/2} d\phi \int_{r_0}^{d/2} r^2 \tau dr \quad , \tag{38}$$

where

$$r_0 = \left(\frac{\cos^2\phi}{a^2} + \frac{\sin^2\phi}{b^2} \right)^{-1/2} \quad . \tag{39}$$

The minus sign is required from the sign convention of Fig.2. If we assume that the plasticity occurs at a constant shearing stress of τ_0, we get

$$\begin{aligned} T_p &= -4\tau_0 \int_0^{\pi/2} d\phi \int_{r_0}^{d/2} r^2 dr & (40) \\ &= -\frac{4\tau_0}{3} \int_0^{\pi/2} \left[\frac{d^3}{8} - \left(\frac{\cos^2\phi}{a^2} + \frac{\sin^2\phi}{b^2} \right)^{-3/2} \right] d\phi & (41) \\ &= -\frac{\pi d^3}{12}\tau_0 + \frac{4a^3\tau_0}{3} \int_0^{\pi/2} (1 - \bar{\mathrm{k}}^2 \sin^2\phi)^{-3/2} d\phi, & (42) \end{aligned}$$

where $\bar{\mathrm{k}}$ is defined as

$$\bar{\mathrm{k}}^2 = 1 - (a/b)^2 = \sin^2\alpha \quad , \tag{43}$$

Since $0 < \bar{\mathrm{k}} < 1$, the positive root is taken.

$$\bar{\mathrm{k}} = \sin\alpha \tag{44}$$

The second term of the right side of T_p is the elliptic integral (Moriguchi et al., 1960; Lebedev, 1972) and $\bar{\mathrm{k}}$ is the modulus of elliptic integral.

$$\int_0^{\pi/2} (1 - \bar{\mathrm{k}}^2 \sin^2\phi)^{-3/2} d\phi = (\frac{b}{a})^2 E(\bar{\mathrm{k}}) \quad , \tag{45}$$

so that

$$T_p = \left[-\frac{\pi d^3}{12} + \frac{4ab^2}{3} E(\bar{\mathrm{k}}) \right] \tau_0 \quad . \tag{46}$$

As a result, a torsion angle is

$$\varphi_T = \frac{(T-T_p)\ell}{G\tilde{I}_p} \tag{47}$$

$$= \left[-X\cos\alpha + \left(\frac{\pi d^3}{12} - \frac{4I_p^3}{3X^3\cos^2\alpha}E(\bar{\mathrm{k}})\right)\tau_0\right]\frac{\ell}{G\tilde{I}_p} \quad . \tag{48}$$

Equating this with Eq.16, we get the equation with respect to X. The equation was solved numerically, since φ_T of Eq.48 includes the elliptic integral. Calculation was done by choosing δ as the controlling variable, as follows.

(i) At a given value of δ, the pitch angle α was determined by Eq.8.

(ii) By equating Eq.16 and 48 and inputting a of Eq.32 and b of Eq.33, the fifth order equation with respect to X was obtained.

$$X^5 + c_4X^4 + c_3X^3 + c_2X^2 + c_1X + c_0 = 0, \tag{49}$$

where

$$c_4 = -\frac{\pi d^3\tau_0}{12\cos\alpha},$$
$$c_1 = \frac{4\pi^3 d^{12}\tau_0^4 E[\bar{\mathrm{k}}]}{3(32)^3\cos^4\alpha},$$
$$c_0 = -\frac{G\pi^5 d^{16}\tau^4\tan\alpha}{R_0(32)^4\cos\alpha(1+\cos^2\alpha)}$$
$$c_3 = c_2 = 0. \tag{50}$$

It was found that the equation had unique solution $X > 0$ for the α varying in the range $[0, \pi/2]$. The solution was obtained numerically by the Newton-Raphson method.

(iii) The radius R was calculated by equating φ_M of Eq.17 with Eq.23,

$$R = \left[\frac{\cos\alpha}{R_0} + \frac{X\sin\alpha}{EI_y}\right]^{-1} \quad . \tag{51}$$

(iv) The load P was calculated through $P = X/R$,

(v) The rotation angle Φ was calculated by Eq.26.

3.5. Approximation of large spring index

The sum of shearing stresses of torsion and simple shear acting on the circular section of wire under the load P is (Wahl, 1963; Shigley, 2015)

$$K\frac{8PD}{\pi d^3} + \frac{4P}{\pi d^2}. \tag{52}$$

The first term is the shearing stress of the torsion of a straight rod multiplied by the curvature correction factor K of Eq.1. Using the index c, the sum is(Wahl, 1963; Shigley, 2015)

$$\frac{8PD}{\pi d^3}\left(1 + \frac{1}{2c}\right). \tag{53}$$

The parenthesis is the factor of the curvature effect.

Conventional springs are designed to have the geometry with the spring index c in the range between 3 and 12(Wahl, 1963; Shigley, 2015; Kobelev, 2018). The index of the piano wire spring, 18.2, was relatively large, which give the factor of Eq.53 equal to 1.027. It suggests that the approximation of taking the factor equal to unity would result in error as large as 2.7 %. In order to simplify the stress analysis, present study shall take the approximation by admitting errors of these magnitude. The validity of the approximation will be judged by comparing the result of calculation with experimental results.

4. Materials and methods

A piano wire, SWP-A grade of JIS (JIS3522, 2014), of d =0.5 mm was used. The straight wire was annealed at 350 °C and was tensile-tested at

Table 1: Dimensions and material properties of piano wire spring

initial coil diameter [mm]	D_0	9.1
wire diameter [mm]	d	0.50
spring index	c	18.2
curvature factor	K	1.08
element length per turn [mm]	ℓ	28.9
number of turns	N	64
initial pitch angle [deg]	α_0	3
flow stress [MPa]	Y	2,000
shearing stress [MPa]	τ_0	1,000
modulus of elasticity [GPa]	E	208
shear modulus [GPa]	G	80
elastic spring constant [Nmm^{-1}]	k	0.84

room temperature with an Instron type testing machine, Shimadzu DSS-500. The stress-strain curve of the specimen with the gauge length of 100 mm is shown in Fig. 5. The elastic limit indicated by an arrow was at 1680 MPa and the flow stress was about 2000 MPa. The elastic-perfect plastic model used for the present calculation is drawn by dotted lines in this figure.

A closely pitched spring of D_0 =9.1 mm was hand-wound and annealed at 350 °C. The spring index $c = D/d$ was 18.2 and the other dimensions are listed in Table 1.

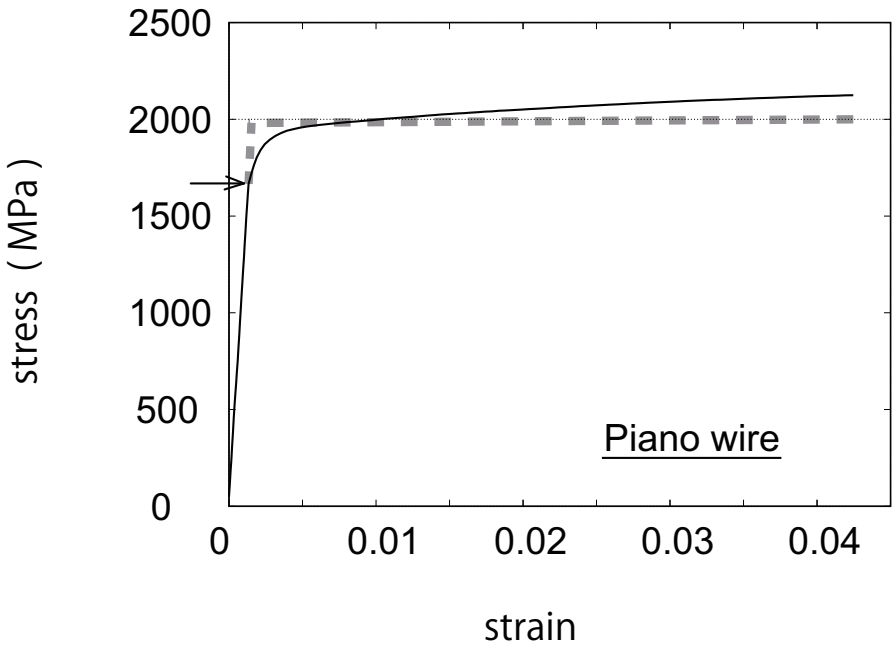

Figure 5: The stress-strain curve of piano wire at room temperature. The elasticity limit indicated by arrow was 1680 MPa. The dotted thick lines are the elastic-perfect plastic model of E =208 GPa and Y =2000 MPa.

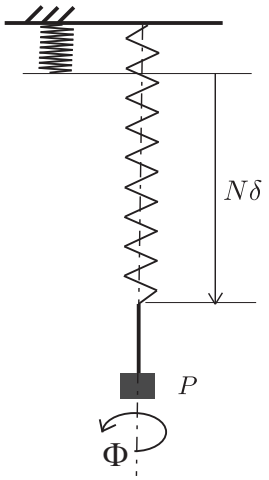

Figure 6: A schematic drawing of the method of loading to spring. The spring was fixed at the upper end and static load was applied to the other end. The deflection and the rotation angle at a given load were measured simultaneously.

5. Results and Discussion

5.1. Deflection of piano wire spring

Load weight was subjected incrementally to the spring. As illustrated in Fig. 6, one end of the spring was fixed to rigid bar and the other was clipped to the cage which can carry a few pieces of weight. As a weight was added to the cage, the displacement of the cage and its rotation angle were measured simultaneously. A protractor was placed beneath the cage. The angle of rotation was large enough to measure by eyes with the protractor.

The piano wire spring was extended up to the weight of P=13 N giving the deflection per pitch δ =25 mm. In order to enlarged views of the load-deflection (P–δ) and the rotation angle-deflection (Φ–δ) curves in the elasticity range are shown in Fig. 7, where δ <12 mm are shown in Fig. 7. In

the two figures the experimental data were plotted by closed circles and the calculated values by lines. The error bars in load are the measure the largest effect of dynamic loading, which is as large as the increment of weight. The increment was 10 g for $P \leq 100$ g, 50 g for or $100 < P \leq 400$ g, and 100 g for $P > 400$ g. The error bars in rotation angle are expressed by

$$\Delta\Phi = 4.93 \times 10^{-3} P \Delta P, \tag{54}$$

which is the first derivative of the equation $\Phi = 2.47 \times 10^{-3} P^2$ derived from Eq.2, 8, and 27 for ν=0.3.

The P–δ relation was linear at the onset of deformation and the slope was in good agreement with Eq.25 for G =80 GPa. The Φ–δ curve was upper concave as similarly to the curve of Eq.27. It is seen that the difference between the theory and experiment increases with increasing δ when δ >4 mm. The yield criterion of Eq.34 indicates the yielding at P=9.1 N for the flow stress of Y=1680 MPa or 10.8 N for Y=2000 MPa. On the other hand, the experimental results showed the deviation from linearity at load as low as 5 N. Such early yielding at small load may be due to microplasticity in hard steels, which occurs by pre-existing mobile dislocations. (Hull and Bacon, 1984; Dieter, 1986).

The P–δ curve of the piano wire spring for large δ is shown in Fig. 8, in which the experimental data are plotted by solid circles. The data points are on the S-shaped curve with the yielding at around P=5 N. The present theory of plastic torsion is plotted as the solid lines with open symbols. The three curves were calculated for the models of elastic-perfect plastic materials with the different magnitude of Y; 1680 MPa, 2000 MPa, and 2400 MPa. It is seen that the experimental data agrees well with the model for Y=2000

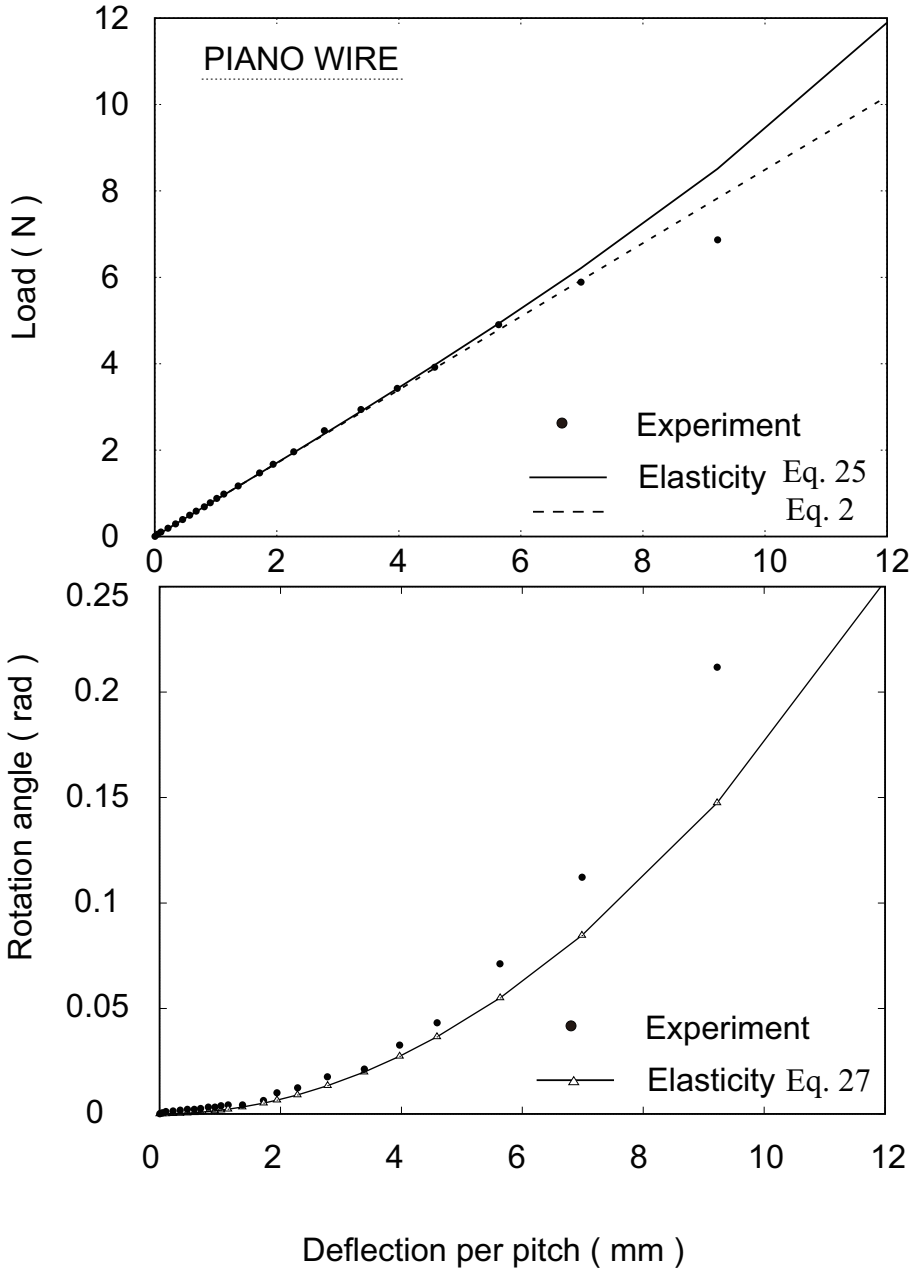

Figure 7: The initial parts of the load–deflection curve and the rotation angle–deflection curve measured simultaneously.

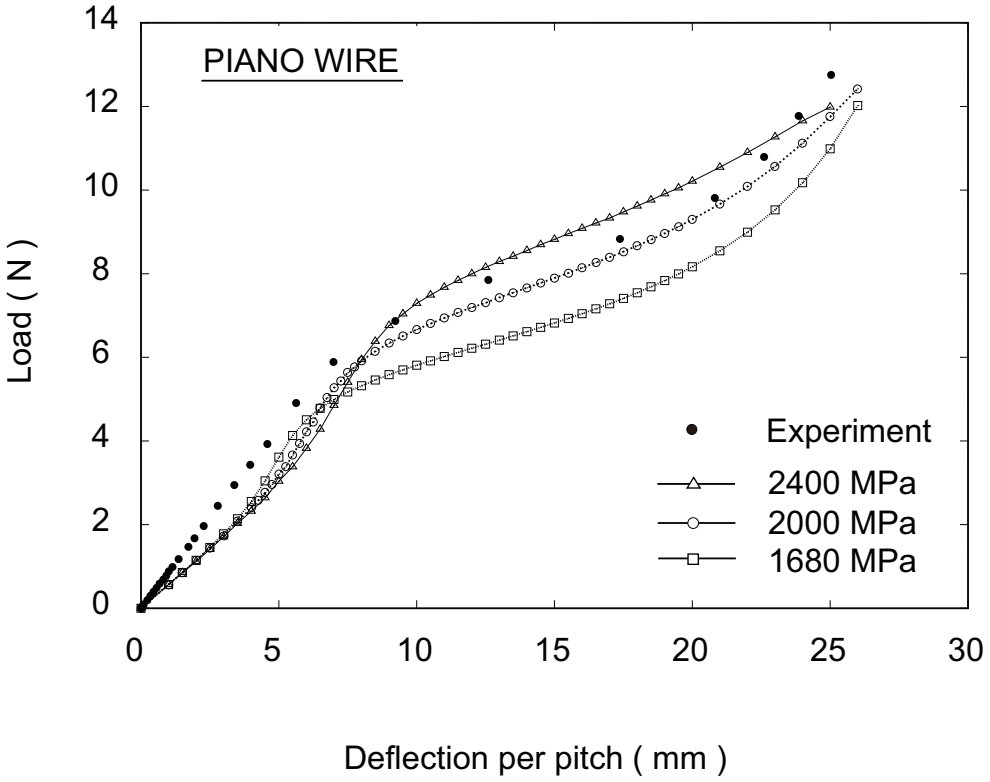

Figure 8: The load–deflection per pitch curve of piano wire spring.

MPa, as seen in Fig. 5. The plasticity theory was out-of-range in elasticity when the deflection was below 5 mm.

The Φ–δ curve is shown in Fig. 9, in which the experimental data are plotted by solid circles. The three curves for different Y were calculated by the present theory of plastic torsion. The dotted line is the present formula in elasticity of Eq.27. These calculated curves show the similar trend with the observed data. It is seen that the rotation angle observed in experiment were bound by the present theories of elasticity and plasticity. The reason why the measured values were smaller than the prediction of plasticity theory

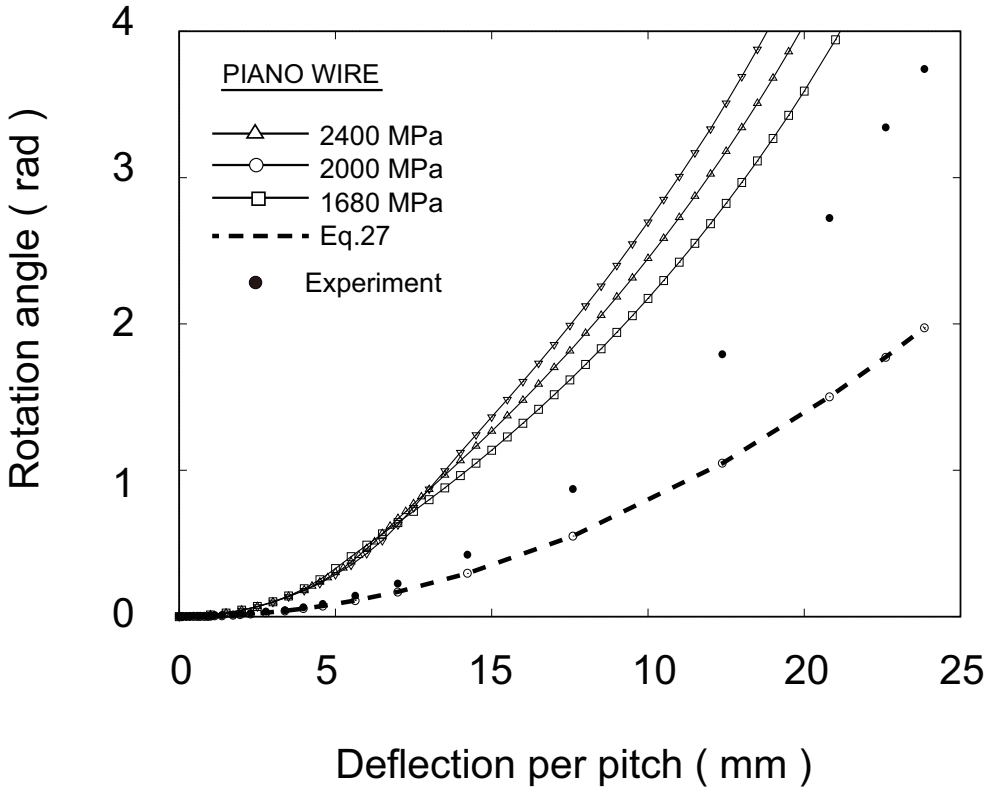

Figure 9: The rotation angle vs deflection per pitch relation in piano wire spring.

is not clear at present. Probable reasons are (i) the effects of microplasticity and/or the residual stress in the piano wire, and (ii) the inertia moment of weight in the experiment.

6. Conclusion

The nonlinear load carrying capacity of helical spring made of elastic-perfect plastic material was examined. A mechanics-of-materials theory was provided by accounting for the combined state of torsion and bending in plasticity under the approximation of large spring index. The moving boundary

problem of tracing the moving yield locus during the plastic torsion was solved. The explicit form of the solution for elastic-perfect plastic material includes the elliptic integral. It was shown that the solutions agreed with the load-deflection curve and the angle of rotation of free end that were measured in the plastic extension of a piano wire spring with the spring index of 18.2.

Acknowledgment

A part of this work was supported by MEXT/JSPS KAKENHI Grant number 19K0498109.

Appendix A.

Let us consider the bending of a curved beam or wire. The radius of curvature ρ_0 and the center angle ϕ_0 are changed to the curvature ρ and the angle ϕ after the bending, as illustrated in Fig. A. As the length of the element is not changed,

$$\rho_0\phi_0 = \rho\phi \tag{A.1}$$

The fiber length at the height z from the centroid axis changes from $(\rho_0+z)\phi_0$ to $(\rho + z)\phi$. The fiber strain is

$$\epsilon = \frac{(\rho + z)\phi}{(\rho_0 + z)\phi_0} - 1 = \frac{z}{\rho_0 + z}\frac{\phi - \phi_0}{\phi_0}. \tag{A.2}$$

Since

$$\frac{\phi}{\phi_0} = \frac{\rho_0}{\rho}, \tag{A.3}$$

and $\rho_0 \gg z$,

$$\epsilon = \frac{z}{\rho_0 + z}\left(\frac{\rho_0}{\rho} - 1\right) \approx z\left(\frac{1}{\rho} - \frac{1}{\rho_0}\right). \tag{A.4}$$

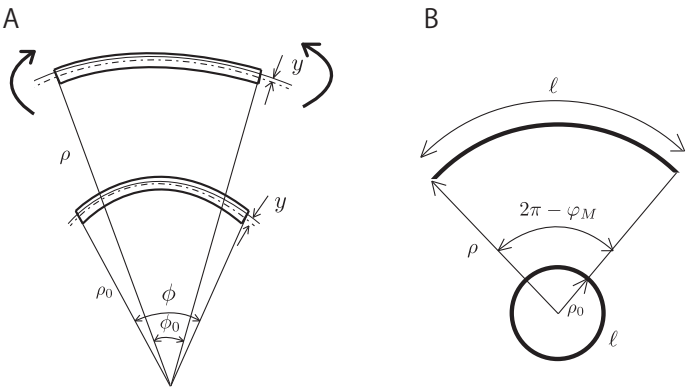

Figure B.10: A; The bending strain in curved beam where the curvature radius is changed from ρ_0 to ρ, B; the change in the shape of a circular ring.

Then, the bending moment is given as

$$\int_A \sigma z dA = E\left(\frac{1}{\rho} - \frac{1}{\rho_0}\right)\int_A z^2 dA \tag{A.5}$$

Defining the moment inertia of area, we get

$$M = E\left(\frac{1}{\rho} - \frac{1}{\rho_0}\right) I_y \tag{A.6}$$

Appendix B.

As illustrated in Fig. B, the element of curved beam with the initial radius of curvature ρ_0 and the center angle ϕ_0 is bent to the curvature ρ and the angle of $2\pi - \varphi_M$.

$$2\pi\rho_0 = (2\pi - \varphi_M)\rho, \tag{B.1}$$

which gives

$$\varphi_M = 2\pi\left(1 - \frac{\rho_0}{\rho}\right) \tag{B.2}$$

References

An, S., Ryu, J., Cho, M., Cho, K., 2012. Engineering design framework for a shape memory alloy coil spring actuator using a static two-state model. Smart Mater & Struct URL: doi/10.1088/0964-1726/21/5/055009.

Burns, S.J., 2011. The relation between helical spring compliance with free and fixed end rotations. J Applied Mechanics 78, 061005. URL: https://doi.org/10.1115/1.4003739.

Dieter, G.E., 1986. Mechanical metallurgy,3rd. McGraw-Hill.

Ge, Q., Qi, H.J., Dunn, M.L., 2013. Active materials by four-dimension printing. Applied Physics Lett. 103. URL: doi//10.1063/1.4819837.

Hull, D., Bacon, D.J., 1984. Introduction to dislocations,3rd. Butterworth-Heinemann.

JIS3522, 2014. Piano wire.

Kobelev, V., 2018. Durability of springs. Springer.

Koh, J., 2018. Design of shape memory alloy coil spring actuator for improving performance in cyclic actuation. Smart Materials & Structures , 2324URL: doi.org//10.3390/ma11112324.

Lebedev, N., 1972. Special functions and their applications. Dover.

Love, A.E.H., 1944. The treatise on the mathematical theory of elasticity, 4th. Dover.

Mirzaeifar, R., Des Roches, R., Yavari, A., 2011. A combined analytical, numerical, and experimental study of shape-memory-alloy helical springs. Int J Solid Struct 48, 611–624. URL: doi.org//0.1016/j.ijsolstr.2010.10.026.

Moriguchi, S., Udagawa, K., Hitotsumatsu, S., 1960. Mathematical formulas vol III. Iwanami Shoten.

Savi, M., Pacheco, P., Garcia, M., Aguiar, R., De Souza, L., Da Hora, R., 2015. Nonlinear geometric influence on the mechanical behavior of shape memory alloy helical spring. Smart Mater & Struct 24. URL: doi.org//10.1088/0964-1726/24/3/035012.

Shigley, J.E., 2015. Mechanical Engineering Design, 10th. McGraw-Hill.

Timoshenko, S.P., Goodier, J., 1970. Theory of elasticity, 3rd. McGraw-Hill.

Tobushi, H., Tanaka, K., 1991. Deformation of a shape memory alloy helical spring. JSME International J. 34, 83–89.

Wahl, A.M., 1963. Mechanical spring, 2nd. McGraw-Hill.